

# Post-growth annealing and wide bandgap modulation of BeZnO layers grown by RF co-sputtering of ZnO and Be targets

J. H. Yu · D. S. Park · J. H. Kim · T. S. Jeong ·  
C. J. Youn · K. J. Hong

Received: 12 March 2009 / Accepted: 15 September 2009 / Published online: 10 November 2009  
© Springer Science+Business Media, LLC 2009

**Abstract** ZnO based oxide system  $\text{Be}_x\text{Zn}_{1-x}\text{O}$  alloy of various compositions has been successfully grown by the RF co-sputtering method. The crystallinity of the  $\text{Be}_x\text{Zn}_{1-x}\text{O}$  alloys has been remarkably improved after the post-annealing at 600 °C compared with the  $\text{Be}_x\text{Zn}_{1-x}\text{O}$  alloys post-annealed at other temperatures. The  $x$  value of the  $\text{Be}_x\text{Zn}_{1-x}\text{O}$  layers has been increased from 0.022 to 0.17 by adjusting the RF-power of the Be target. Also, the optical bandgap energy has been modulated from 3.2218 to 3.7978 eV, respectively. Based on our results, a bandgap bowing parameter of  $\text{Be}_x\text{Zn}_{1-x}\text{O}$  alloy has been extracted out to be 4.5 eV. These findings could be useful to fabricate the ZnO/ $\text{Be}_x\text{Zn}_{1-x}\text{O}$  quantum structures and bandgap modulation for deep ultraviolet-light-emitting diodes.

## Introduction

ZnO-based oxides such as MgZnO, CdZnO, and BeZnO are the most promising oxides for photonic and electronic applications to compete with GaN-based devices [1]. It is necessary to produce high-efficiency ZnO devices that need the fabrication of ZnO-based quantum wells (QWs) and superlattice structure. Such structure could be used to fabricate ZnO-based alloys with bandgaps larger or smaller than that of ZnO. A first approach for fabrication of QW

structures was the ternary  $\text{Mg}_x\text{Zn}_{1-x}\text{O}$  alloy [2]. The 3.99 eV bandgap energy of the  $\text{Mg}_x\text{Zn}_{1-x}\text{O}$  has been reported at room temperature when the content of Mg is increased up to  $x = 0.33$  [2]. However, the Mg constituent in  $\text{Mg}_x\text{Zn}_{1-x}\text{O}$  is larger than  $x > 0.36$ , the crystal phase segregation and thermal instability were observed due to the different crystal structure and large lattice mismatch between ZnO (3.25 Å, hexagonal) and MgO (4.22 Å, cubic) [3].

Recently, Ryu et al. [4] have suggested  $\text{Be}_x\text{Zn}_{1-x}\text{O}$  as a candidate for achieving the bandgap modulation to values larger than that of ZnO. The crystal structure of ZnO and BeO are both hexagonal. BeO is a wide bandgap,  $E_g = 10.6$  eV, oxide material [5]. The  $\text{Be}_x\text{Zn}_{1-x}\text{O}$  alloy films can be easily synthesized by mixing ZnO with Be. Also, no phase segregation was observed between ZnO and BeO when the Be concentration is varied over the entire range from 0 to 100% [4]. Therefore, the  $\text{Be}_x\text{Zn}_{1-x}\text{O}$  alloy has been to avoid such problems observed in the  $\text{Mg}_x\text{Zn}_{1-x}\text{O}$  alloy used for a potential barrier layer in the QW structure [4]. This indicated that the  $\text{Be}_x\text{Zn}_{1-x}\text{O}$  alloy film be potentially a strong candidate for the development of the ZnO-based ultraviolet (UV) light-emitting-diodes (LEDs). Furthermore, Ding et al. [6] calculated the bowing parameter on the theoretical bandgap tuning of  $\text{Be}_x\text{Zn}_{1-x}\text{O}$  alloys using ab initio simulations. For the ternary compound semiconductor, the bandgap energy,  $E_{\text{BeZnO}}$ , can be expressed by empirical equation [7]:

$$E_{\text{BeZnO}}(x) = (1-x)E_{\text{ZnO}} + xE_{\text{BeO}} - bx(1-x), \quad (1)$$

where  $b$  is the bowing parameter and  $E_{\text{ZnO}}$  and  $E_{\text{BeO}}$  are the bandgap energies of compounds ZnO and BeO of the compound  $\text{Be}_x\text{Zn}_{1-x}\text{O}$ , respectively.

In this study, RF co-sputtering has been successfully used to grow  $\text{Be}_x\text{Zn}_{1-x}\text{O}$  alloy through ZnO and Be targets.

J. H. Yu · D. S. Park · J. H. Kim · T. S. Jeong · C. J. Youn (✉)  
Semiconductor Physics Research Center (SPRC), School  
of Semiconductor and Chemical Engineering, Chonbuk National  
University, Jeonju 561-756, South Korea  
e-mail: cjyoun@chonbuk.ac.kr

K. J. Hong  
Department of Physics, Chosun University, Gwangju 501-759,  
South Korea

The Be mole fraction,  $x$ , in the  $\text{Be}_x\text{Zn}_{1-x}\text{O}$  was controlled by adjusting the RF powder of the Be target. The variation of the Be composition in the grown  $\text{Be}_x\text{Zn}_{1-x}\text{O}$  alloy was carried with varying the post-annealing temperature. Based on these results, post-annealing effect and bandgap modulation on  $\text{Be}_x\text{Zn}_{1-x}\text{O}$  were also discussed.

## Experimental procedure

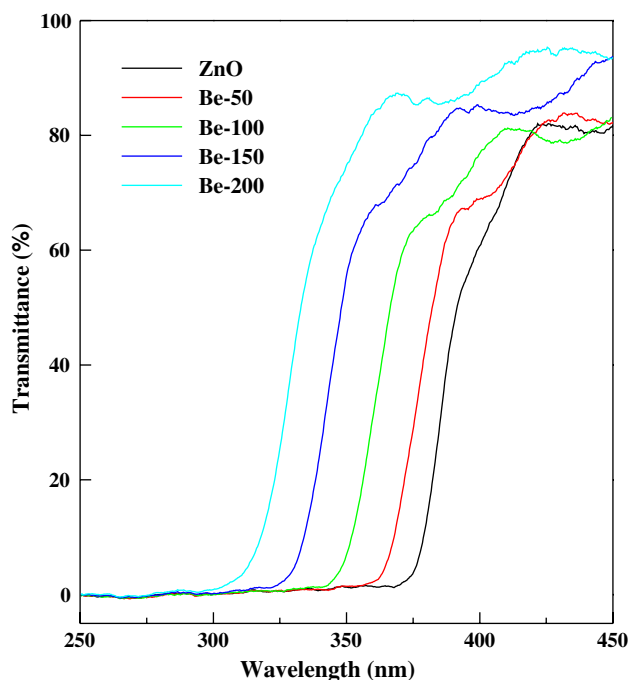
$\text{BeZnO}$  layers were grown using a commercial RF magnetron sputtering system (Aja International Inc., USA) with an automatic matching network. A ZnO (5 N, KURT, USA) and Be (3 N, ESL, CHINA) targets of 2-inch diameter was loaded into the sputtering chamber. In order to have a uniform layer thickness, the rotating speed of the substrate was kept at 40 rpm during the deposition. The target–substrate distance was set at 10 cm. The substrate used for the  $\text{BeZnO}$  layers was (0001)  $\text{Al}_2\text{O}_3$ . The base pressure was evacuated to a pressure lower than  $5 \times 10^{-8}$  Torr. Prior to  $\text{BeZnO}$  layer growth, the surface of the substrate was cleaned with acetone and ethanol for 5 min and was etched in  $\text{H}_2\text{SO}_4:\text{H}_2\text{PO}_4 = 3:1$  for 7 min. Then, it was rinsed in deionized water. The loaded target was continuously pre-sputtered for 30 min under a 50-W RF power to remove any surface contamination of the target. In order to grow  $\text{Be}_x\text{Zn}_{1-x}\text{O}$  layers, ZnO and Be targets were sputtered together. RF power of ZnO target was set at 150 W and the Be flux was controlled by varying the RF power of the Be target. These powers were 0, 50, 100, 150, and 200 W (Hereafter, the powers of the Be target will be labeled as ZnO, Be-50, -100, -150, and -200, respectively). During  $\text{Be}_x\text{Zn}_{1-x}\text{O}$  layer growth, the flows of Ar and  $\text{O}_2$  were controlled in 10 and 40 sccm, respectively, to create ambient pressure as background flows. At this time, the substrate temperature and the working pressure were set at 150 °C and 4 mTorr, respectively. Under these conditions, the thickness of the grown  $\text{Be}_x\text{Zn}_{1-x}\text{O}$  layers was about 580 nm. After growth, post-annealing of the grown samples were carried out in a rapid thermal annealing (RTA) system at temperatures ranging from 500 to 1000 °C for 30 s in  $\text{N}_2$  ambient to achieve the crystallization of the  $\text{Be}_x\text{Zn}_{1-x}\text{O}$  alloy. Nevertheless, it is rather difficult to obtain the precise Be concentration in the  $\text{Be}_x\text{Zn}_{1-x}\text{O}$  alloy films due to the absence of the standard layer sample and large uncertainty of detecting the light Be element. In order to confirm the existence of the Be content, the mini-SIMS (Mill Brook) experiment was performed. The mini-SIMS was analyzed by using  $\text{Ga}^+$  source at the energy of 6 kV and the beam current of 3 nA. Therefore, the Be composition in the  $\text{Be}_x\text{Zn}_{1-x}\text{O}$  was estimated by comparing the X-ray diffraction (XRD) and mini-SIMS. The crystal quality of the  $\text{Be}_x\text{Zn}_{1-x}\text{O}$  layers was estimated by XRD, scanning electron microscopy (SEM),

and atomic force microscopy (AFM). The optical transmission spectra were investigated with an UV visible infrared spectrometer.

## Results and discussion

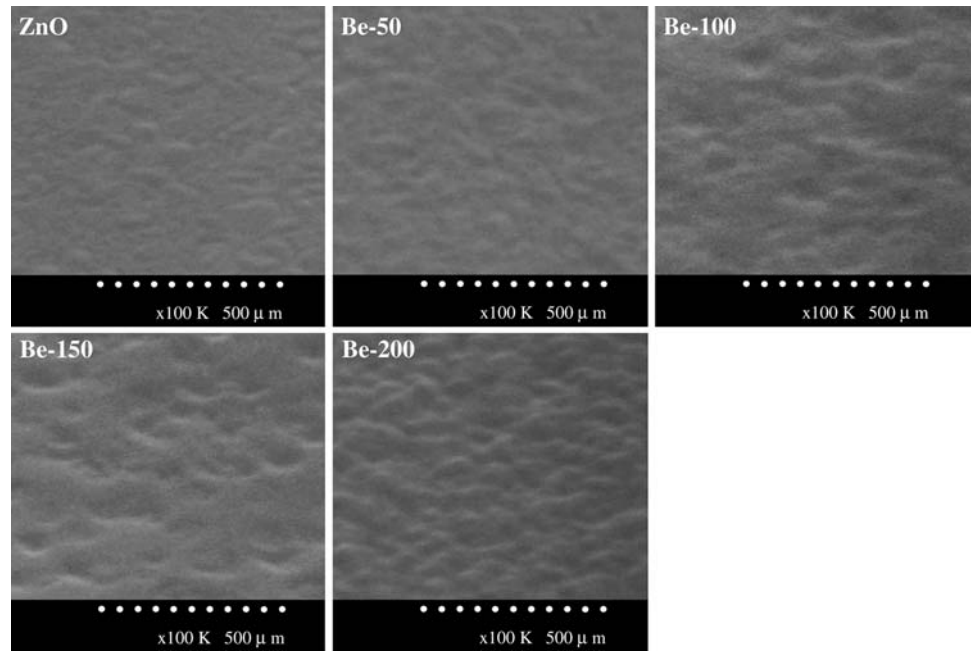
### Post-growth annealing by means of RTA

Figure 1 shows the optical transmission spectra on the as-grown  $\text{Be}_x\text{Zn}_{1-x}\text{O}$  layers obtained by varying the RF power of the Be target. The figure shows that the cut-off wavelength on the transmittance spectra shifted toward the short-wavelength region. This indicates that the concentration of Be atoms in the  $\text{Be}_x\text{Zn}_{1-x}\text{O}$  layer increase with raising the RF power of the Be target and are well mixed. Figure 2 displays the surface morphologies of as-grown  $\text{Be}_x\text{Zn}_{1-x}\text{O}$  layers by the SEM measurement. As shown in Fig. 2, the surface roughness of as-grown  $\text{Be}_x\text{Zn}_{1-x}\text{O}$  layers rose steeply with increasing RF power of the Be target. The intermixing of Be atoms in ZnO is thought to be interrupted as the increase of the Be elements. Also, this phenomenon leads to the reduction of the growth rate. Therefore, in order to grow the same thickness of the  $\text{Be}_x\text{Zn}_{1-x}\text{O}$  layer, the growth time in the high RF power of the Be target was prolonged. After the growth, the post-growth annealing (hereafter, a sentence of the post-growth annealing will be written to post-annealing) was carried out at the temperature range from 500 to 1000 °C to

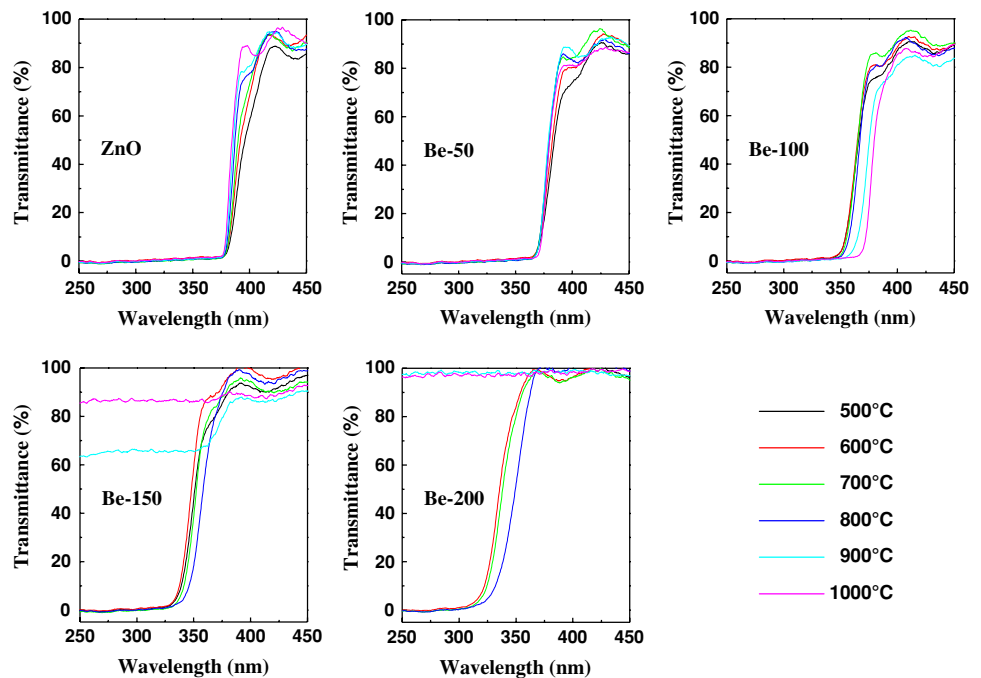


**Fig. 1** Optical transmission spectra on the as-grown  $\text{Be}_x\text{Zn}_{1-x}\text{O}$  layers obtained by varying the RF power of the Be target

**Fig. 2** Surface morphologies of as-grown  $\text{Be}_x\text{Zn}_{1-x}\text{O}$  layers by the SEM measurement



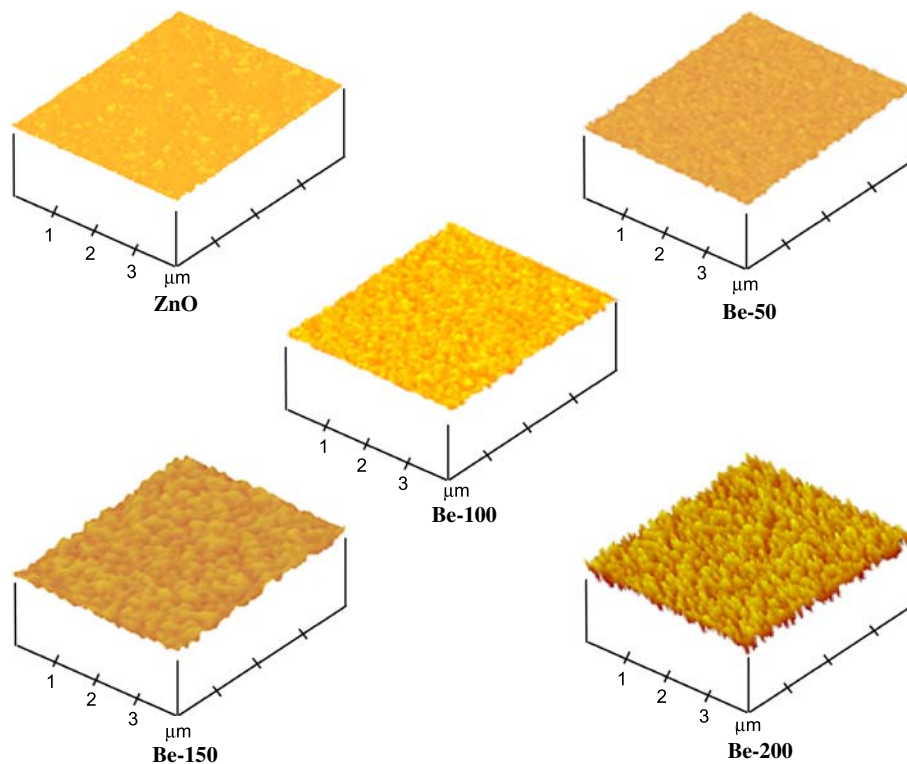
**Fig. 3** Optical transmission spectra on the  $\text{Be}_x\text{Zn}_{1-x}\text{O}$  layers obtained from the temperature ranging from 500 to 1000 °C. Here, the transmittance spectra of each figure displayed as a relation of the temperature variation on the post-annealing of the as-grown  $\text{Be}_x\text{Zn}_{1-x}\text{O}$  layers, which was grown by varying the RF power of the Be target



enhance the crystallization on the  $\text{Be}_x\text{Zn}_{1-x}\text{O}$  layers. Figure 3 shows the optical transmission spectra on the  $\text{Be}_x\text{Zn}_{1-x}\text{O}$  layers obtained from the temperature ranging from 500 to 1000 °C. Each figure shows that the transmittance spectra of the  $\text{Be}_x\text{Zn}_{1-x}\text{O}$  layers are displayed as a variation of the post-annealing temperature. The cut-off wavelength on the post-annealing sample of 600 °C shifted toward the higher energy side. However, the samples grown with high RF power showed that the cut-off

wavelength shifted toward the lower energy side after the post-annealing between 700 and 1000 °C. Furthermore, the surfaces on layers annealed at 900 and 1000 °C were observed to be destroyed. This is associated to the decrease of the crystalline quality due to the higher post-annealing temperature than the reasonable temperature to mix Be atoms in the ZnO layer. Therefore, the Be atoms textured in the  $\text{Be}_x\text{Zn}_{1-x}\text{O}$  layer are to be diffused out rather than to be mixed into the layer in the high post-annealing.

**Fig. 4** AFM surface-morphologies on the  $\text{Be}_x\text{Zn}_{1-x}\text{O}$  layers post-annealed at 600 °C



Consequently, the good crystalline quality in the post-annealing samples of 600 °C was obtained. Figure 4 shows the AFM surface-morphologies on the  $\text{Be}_x\text{Zn}_{1-x}\text{O}$  layers post-annealed at 600 °C. The ZnO, Be-50, and Be-100 samples show that the root-mean-square values,  $R_{\text{ms}}$ , of the surface roughness were 1.89, 3.09, and 3.17 nm, respectively. However, the Be-150 and Be-200 samples show that surface morphologies are comparatively rough and the  $R_{\text{ms}}$  values were 5.33 and 7.11 nm, respectively. This suggests to be primarily caused by the interaction increase between ZnO and Be flux as the RF power is increased. Figure 5 presents the XRD spectra on the  $\text{Be}_x\text{Zn}_{1-x}\text{O}$  layers post-annealed at 600 °C. These patterns correspond to the diffraction peaks of the ZnO (0002),  $\text{Be}_x\text{Zn}_{1-x}\text{O}$  (0002), and  $\text{Al}_2\text{O}_3$  (0006). As shown in Fig. 5, the (0002) diffraction peak of ZnO shifted to a high diffraction angle owing to the Be concentration in the  $\text{Be}_x\text{Zn}_{1-x}\text{O}$  alloy. This indicates that the layers are strongly oriented to the  $c$ -axis of the hexagonal structure and also epitaxially crystallized under constraints created by the substrate. According to Vegard’s law, the  $x$  value in the  $\text{Be}_x\text{Zn}_{1-x}\text{O}$  layer was extracted out. For the layers of Be-50, -100, -150, and -200, the  $x$  rates of  $\text{Be}_x\text{Zn}_{1-x}\text{O}$  were estimated to be 0.022, 0.066, 0.116, and 0.17, respectively. Figure 6 shows the mini-SIMS spectra on the  $\text{Be}_x\text{Zn}_{1-x}\text{O}$  layers post-annealed at 600 °C. As shown in Fig. 6, the peak intensity of the Be component tends to be strongly enhanced with the increasing the RF power of the Be target. The XRD and mini-SIMS results led us to conclude that the Be content is substituted for the host-lattice site in ZnO.

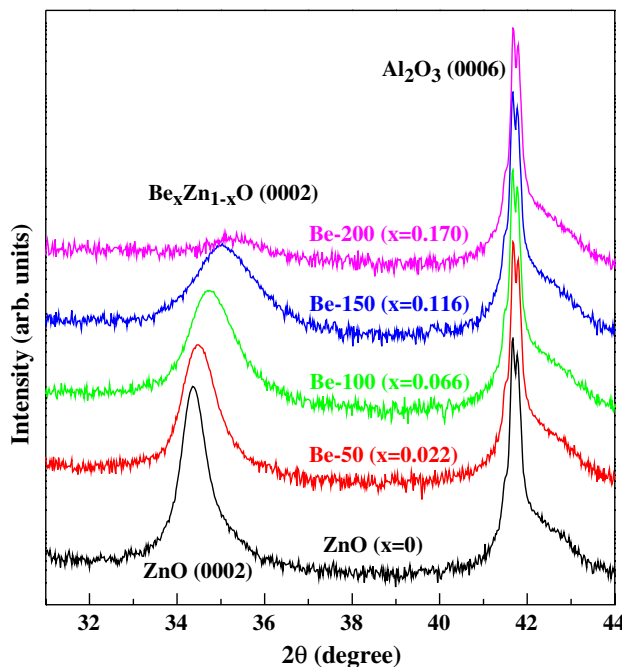


**Fig. 5** XRD spectra on the  $\text{Be}_x\text{Zn}_{1-x}\text{O}$  layers post-annealed at 600 °C

Bandgap modulation on  $\text{Be}_x\text{Zn}_{1-x}\text{O}$  layers

Figure 7 displays the optical transmission spectra on the  $\text{Be}_x\text{Zn}_{1-x}\text{O}$  layers post-annealed at 600 °C. This shows that the transmittance spectra exist in the UV region ranging

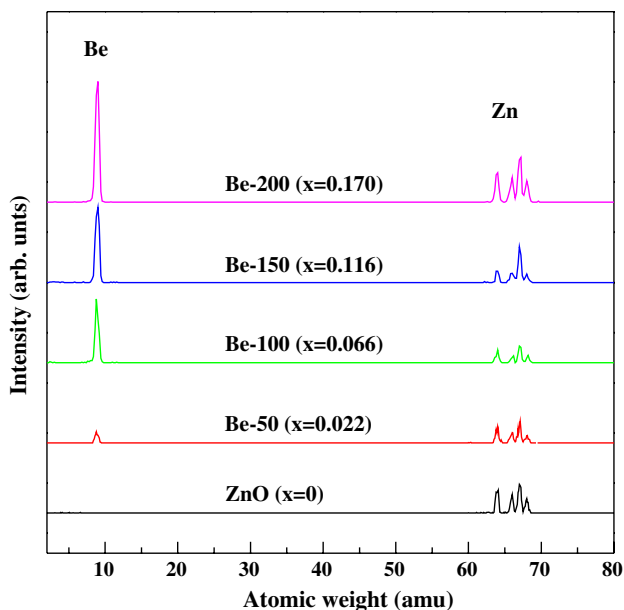


**Fig. 6** Mini-SIMS spectra on the  $\text{Be}_x\text{Zn}_{1-x}\text{O}$  layers post-annealed at  $600^\circ\text{C}$

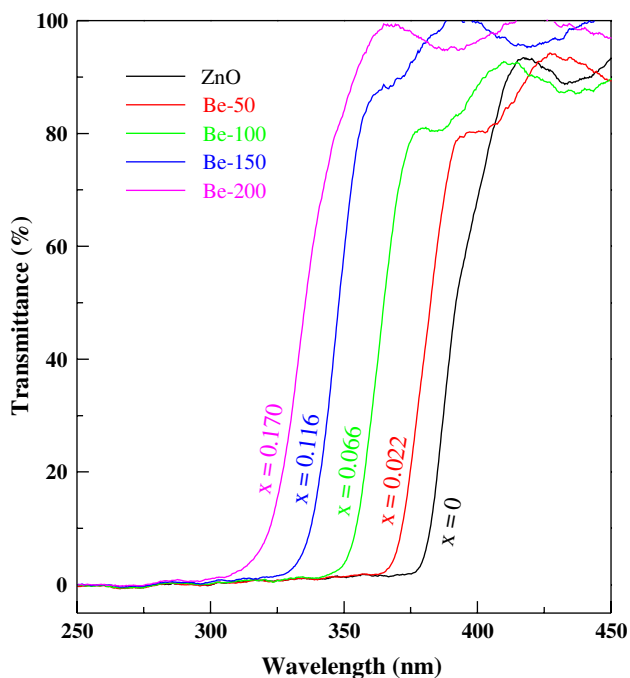


**Fig. 7** Optical transmission spectra on the  $\text{Be}_x\text{Zn}_{1-x}\text{O}$  layers post-annealed at  $600^\circ\text{C}$

from 300 to 400 nm according to the various  $x$  values. Also, the transmittance rate was improved to be more than 90% after the post-annealing. This high transmittance is associated with the reduction of scattering and absorption due to the improvement of crystal quality. The absorption coefficients can be calculated from the transmission spectra in the

UV region. Therefore, the relation between transmittance ( $T$ ) and absorption coefficient ( $\alpha$ ) can be expressed as

$$\alpha = (\ln T^{-1})/d, \quad (2)$$

where  $d$  is the thickness of the layer. Also, the model for direct inter-band transitions is generally used to determine the bandgap energy:

$$(\alpha h\nu)^2 = A(h\nu - E_g), \quad (3)$$

where  $A$  is a function of refractive index and hole/electron effective masses, and  $h\nu$  is the energy of the incident photon. Figure 8 shows the plot of  $(\alpha h\nu)^2$  as a function of photon energy on the  $\text{Be}_x\text{Zn}_{1-x}\text{O}$  layers obtained by the Vegard's law. The bandgap energy can be evaluated from the intercept of the extrapolated linear part of the curve with the energy axis. As shown in Fig. 8, the optical bandgap energy shifts from 3.2218 to 3.7978 eV with increasing Be concentration due to the RF power of the Be target. Figure 9 presents the bandgap energies of the  $\text{Be}_x\text{Zn}_{1-x}\text{O}$  layers as a function of the Be-concentration  $x$ . Using Eq. 1, the relationship between  $x$  and bandgap can be empirically obtained as

$$E_{\text{BeZnO}}(x) = 4.5(x - 1)x + 7.3782x + 3.2218, \quad (4)$$

where  $E_{\text{ZnO}}$  and  $E_{\text{BeO}}$  are 3.2218 and 10.6 eV, respectively. In this equation, the bandgap bowing parameter of  $\text{Be}_x\text{Zn}_{1-x}\text{O}$  is 4.5 eV. However, this value is very small comparing with the 5.6 eV obtained from the theoretical fitting of  $\text{Be}_x\text{Zn}_{1-x}\text{O}$  alloys [6]. Therefore, this finding is

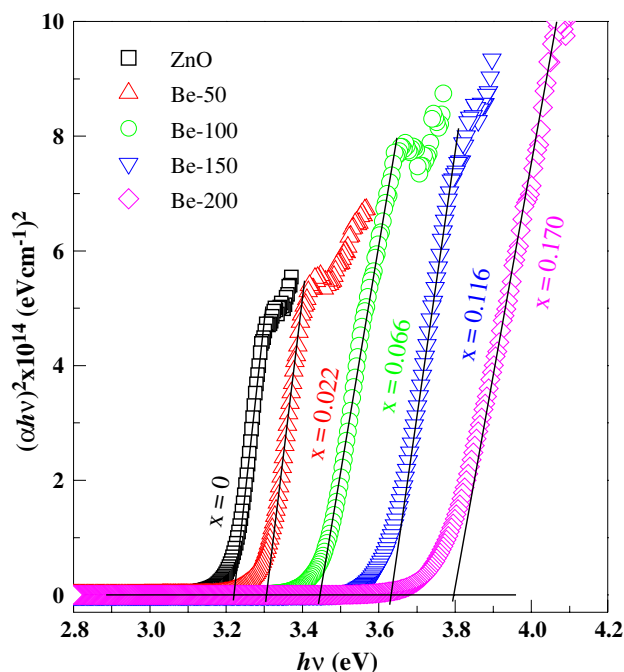


**Fig. 8** Plot of  $(\alpha h\nu)^2$  as a function of photon energy on the  $\text{Be}_x\text{Zn}_{1-x}\text{O}$  layers obtained by the Vegard's law

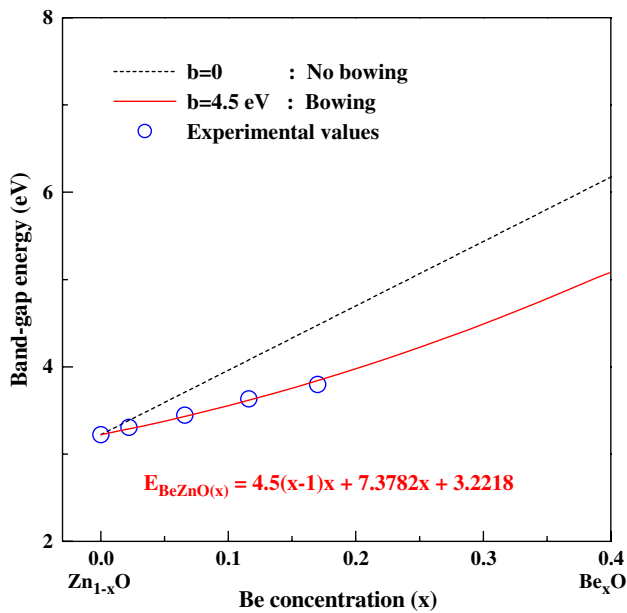


**Fig. 9** Bandgap energies of the  $\text{Be}_x\text{Zn}_{1-x}\text{O}$  layers as a function of the Be-concentration  $x$

required to be more accurate value based on the experiments to apply for the  $\text{Be}_x\text{Zn}_{1-x}\text{O}$  bandgap engineering. Also, it is worth noting that the  $\text{Be}_x\text{Zn}_{1-x}\text{O}$  layers can be used as potential barrier layers in active layers consisting of the  $\text{ZnO}/\text{Be}_x\text{Zn}_{1-x}\text{O}$  quantum well structure through the bandgap modulation by alloying  $\text{ZnO}$  with  $\text{Be}$ .

## Conclusion

A wide bandgap  $\text{Be}_x\text{Zn}_{1-x}\text{O}$  alloy has been successfully grown by the RF co-sputtering method through  $\text{ZnO}$  and  $\text{Be}$  target. The  $\text{Be}$  contents in  $\text{Be}_x\text{Zn}_{1-x}\text{O}$  alloy can be

varied by adjusting the RF power of the  $\text{Be}$  target. Effect of post-growth annealing on the structural and optical properties of the  $\text{Be}_x\text{Zn}_{1-x}\text{O}$  alloys was systematically investigated. The increase of the  $\text{Be}$  loss in the  $\text{Be}_x\text{Zn}_{1-x}\text{O}$  alloys was observed by increasing the temperature of post-annealing. The crystal quality of the  $\text{Be}_x\text{Zn}_{1-x}\text{O}$  alloys post-annealed at  $600^\circ\text{C}$  was remarkably improved in comparison with that of the  $\text{BeZnO}$  alloys at other temperatures. The  $x$  rates of the  $\text{Be}_x\text{Zn}_{1-x}\text{O}$  layer were estimated to be 0.022, 0.066, 0.116, and 0.17, respectively, with increasing the RF power of  $\text{Be}$  target. Also, the corresponding optical bandgap energy was obtained ranging from 3.2218 to 3.7978 eV. Based on our results, a bandgap bowing parameter of 4.5 eV was derived.

**Acknowledgement** This work was supported by the Korea Research Foundation Grant funded by the Korean Government (KRF-2008-005-J00302).

## References

1. Chang SP, Chang SJ, Chiou YZ, Lu CY, Lin TK, Lin YC, Kuo CF, Chang HM (2007) *J Electrochem Soc* 154:J209
2. Ohtomo A, Kawasaki M, Koida T, Masubuchi K, Koinuma H, Sakurai Y, Yoshida Y, Yasuda T, Segawa Y (1998) *Appl Phys Lett* 72:2466
3. Choopun S, Vispute RD, Yang W, Sharma RP, Venkatesan T, Shen H (2002) *Appl Phys Lett* 80:1529
4. Ryu YR, Lee TS, Lubguban JA, White HW, Leem JH, Han MS, Park YS, Youn CJ, Kim WJ (2006) *Appl Phys Lett* 88:052103
5. Waag A, Fischer F, Lugauer HJ, Litz Th, Laubender J, Lenz U, Zehnder U, Ossau W, Gerhardt T, Möller M, Landwehr G (1996) *J Appl Phys* 80:792
6. Ding SF, Fan GH, Li ST, Chen K, Xiao B (2007) *Physica B* 394:127
7. Van Vechten JA, Bergstresser TK (1970) *Phys Rev B* 1:3351